

UCLA

UCLA Previously Published Works

Title

Visual Input to the Drosophila Central Complex by Developmentally and Functionally Distinct Neuronal Populations

Permalink

<https://escholarship.org/uc/item/2zc9m5sk>

Journal

Current Biology, 27(8)

ISSN

0960-9822

Authors

Omoto, Jaison Jiro
Keleş, Mehmet Fatih
Nguyen, Bao-Chau Minh
[et al.](#)

Publication Date

2017-04-01

DOI

10.1016/j.cub.2017.02.063

Peer reviewed



Published in final edited form as:

Curr Biol. 2017 April 24; 27(8): 1098–1110. doi:10.1016/j.cub.2017.02.063.

Visual input to the *Drosophila* central complex by developmentally and functionally distinct neuronal populations

Jaison Jiro Omoto^{a,1}, Mehmet Fatih Kele^{b,1}, Bao-Chau Minh Nguyen^a, Cheyenne Bolanos^a, Jennifer Kelly Lovick^a, Mark Arthur Frye^{b,c,*}, and Volker Hartenstein^a

^aDepartment of Molecular, Cell and Developmental Biology, University of California, Los Angeles, Los Angeles, CA 90095, USA

^bDepartment of Integrative Biology and Physiology, University of California, Los Angeles, Los Angeles, CA 90095, USA

Summary

The *Drosophila* central brain consists of stereotyped neural lineages, developmental-structural units of macrocircuitry formed by the sibling neurons of single progenitors called neuroblasts. We demonstrate that the lineage principle guides the connectivity and function of neurons providing input to the central complex, a collection of neuropil compartments important for visually-guided behaviors. One of these compartments is the ellipsoid body (EB), a structure formed largely by the axons of ring (R) neurons, all of which are generated by a single lineage, DALv2. Two further lineages, DALc1 and DALc2, produce neurons that connect the anterior optic tubercle, a central brain visual center, with R neurons. Finally, DALc1/2 receives input from visual projection neurons of the optic lobe medulla, completing a three-legged circuit we call the anterior visual pathway (AVP). The AVP bears fundamental resemblance to the sky-compass pathway, a visual navigation circuit described in other insects. Neuroanatomical analysis and two-photon calcium imaging demonstrates that DALc1 and DALc2 form two parallel channels, establishing connections with R neurons located in the peripheral and central domains of the EB, respectively. Although neurons of both lineages preferentially respond to bright objects, DALc1 neurons have small ipsilateral, retinotopically-ordered receptive fields, whereas DALc2 neurons share a large excitatory receptive field in the contralateral hemifield. DALc2 neurons become inhibited when the object enters the ipsilateral hemifield, and display an additional excitation after the object leaves the field of view. Thus, the spatial position of a bright feature, such as a celestial body, may be encoded within this pathway.

*Corresponding to: volkerh@mcdb.ucla.edu (V. Hartenstein), frye@ucla.edu (M.A. Frye).

^cLead Contact: frye@ucla.edu (M.A. Frye)

¹Equal Contribution

Author Contributions

Conceptualization, J.J.O, M.F.K, M.A.F, V.H.; Methodology, J.J.O, M.F.K.; Formal analysis, M.F.K; Investigation, J.J.O, M.F.K, B.M.N., C.B., J.K.L.; Writing – Original Draft, J.J.O, M.F.K, M.A.F, V.H.; Visualization, J.J.O, M.F.K, M.A.F, V.H.; Supervision and Funding Acquisition – M.A.F, V.H.

Publisher's Disclaimer: This is a PDF file of an unedited manuscript that has been accepted for publication. As a service to our customers we are providing this early version of the manuscript. The manuscript will undergo copyediting, typesetting, and review of the resulting proof before it is published in its final citable form. Please note that during the production process errors may be discovered which could affect the content, and all legal disclaimers that apply to the journal pertain.

Introduction

The central complex (CX) is an evolutionarily conserved domain in the insect brain that has a highly ordered, modular neuronal architecture. In *Drosophila*, it comprises several compartments that are situated across the brain midline, including (from anterior to posterior), the ellipsoid body (EB), fan-shaped body (FB) with noduli (NO), and protocerebral bridge (PB) [1–3]. The ellipsoid body is flanked laterally by two compartments of the lateral complex, the bulb (BU) and lateral accessory lobe (LAL), which act as portals for input to and output from the central complex.

Numerous anatomical, functional, and genetic studies conducted in the past suggest that the central complex is involved, among other functions, in the control of motor output and spatial orientation. Stimulation of the CX alters a large number of behaviors that require fine motor control, including stridulation, walking, and escape [4,5]. Genetic lesions of the CX affect walking and flight [6,7]. Silencing specific classes of ring neurons innervating the ellipsoid body of the CX causes deficits in visual place learning and spatial orientation memory in *Drosophila* [8,9]. Along these lines, functional imaging studies in behaving flies suggest that populations of columnar neurons in the CX encode the fly's spatial orientation relative to its environment [10], suggesting that the CX could play a navigational role similar to that one of the hippocampus and entorhinal cortex in mammals [11].

Similar to the mushroom body, another highly structured neuropil domain of the insect brain known for its pivotal function in olfactory learning and memory, the central complex does not receive direct input from peripheral sense organs. Processed sensory information is relayed from the primary olfactory center (antennal lobe) to the mushroom body and superior protocerebrum *via* antennal lobe projection neurons. These anatomically and functionally specialized neurons are derived from four developmentally defined classes, so called lineages [12,13]. A lineage comprises all neurons produced by a single neural progenitor (neuroblast). The fly brain is generated by approximately 100 pairs of such neuroblasts, each of which defined by a unique pattern of gene expression that dictates the morphology and function of the cells within the lineage [14]. Its lineage-based composition provides great conceptual and technical advantages to analyze the structure and development of the antennal lobe projection in great detail, making this input pathway one of the preeminent model systems to study the genetic mechanism controlling the assembly of a central brain circuit [15,16].

By comparison to the antennal lobe input pathway towards the mushroom body, very little is known about the circuitry providing input to the *Drosophila* central complex. It must receive input from the visual system; dendrites of ellipsoid body ring (R) neurons, located in the bulb, are sensitive to visual stimuli and form a retinotopically-ordered arrangement [17]. In other insects, neurons conducting visual information from the optic lobe to the CX have been characterized, using anatomical and electrophysiological methods, in considerable detail [18]. This circuit, called the sky-compass pathway, is thought to encode skylight cue information relevant for navigation, such as the spatial position of bright celestial bodies, the pattern of polarized skylight, or the sky's spectral gradient. It is a pathway consisting of multiple layers; neurons of the optic lobe medulla project to a known domain of visual input

in the central brain called the anterior optic tubercle (AOTU). From there, information is relayed by another neuronal population to the bulb, the input domain of tangential neurons which arborize in the central body lower division (homologous to *Drosophila* ring neurons and ellipsoid body) [19–24].

In this paper, we have investigated the visual input pathway to the central complex in *Drosophila*. Which, if any, lineages form the “building blocks” of this pathway? Does the lineage principle guide the structural connectivity and thus, the function of neuronal circuit elements within this pathway? Using clonal analysis, we and others previously identified the projection pattern for the majority of neuroblast lineages in the *Drosophila* brain [25–28]. This analysis revealed that ring (R) neurons of the ellipsoid body are derived from a single paired lineage (DALv2). Two additional lineages (DALcl1 and 2) were identified; similarly to neurons in the sky-compass pathway, they project from the anterior optic tubercle to the bulb, and we thus call them tuberculo-bulbar (TuBu) neurons. Identification of Gal4 drivers which reflect the projection pattern of neurons within these lineages allowed us to demonstrate a parallel pattern of topographically-ordered connectivity within this pathway. Double labeling and GFP reconstitution across synaptic partners (GRASP) demonstrates that TuBu neurons provide direct input to R neurons. Two-photon calcium imaging of TuBu neuron presynaptic terminals further corroborates this notion; TuBu neuron outputs from DALcl1, which predominantly innervate the superior domain of the bulb, exhibit similar response properties as R neuron dendrites from the same region, based on previous studies [17]. However, DALcl2 TuBu neuron outputs, which predominantly innervate the inferior domain of the bulb, do not respond in the same fashion, demonstrating that the lineage principle determines not only the structure, but also the function of neuronal populations.

Results

Discrete neural lineages form input pathways of the ellipsoid body

The pathway providing input from the optic lobe to the ellipsoid body, called the anterior visual pathway (AVP) in the following (Fig. 1A), represents a circuit whose central part is formed by the neurons of three lineages. As known from previous works and summarized above, ring (R) neurons of lineage DALv2 project from the bulb to the ellipsoid body. Cell bodies of this lineage are located in the anterior brain cortex, surrounding the spur of the mushroom body. The bulb receives the short, proximal neurites of DALv2 neurons; DALv2 axons form a fiber tract, termed the anterior lateral ellipsoid body tract (LEa), which extends medially towards the EB (Fig. 1B) [2,29].

We identified two hemilineages, DALcl1d and DALcl2d, which interconnect the bulb with the anterior optic tubercle (AOTU) *via* tuberculo-bulbar (TuBu) neurons (Fig. 1C, D). The identified neurons resemble likely homologs, called tubercle-lateral accessory lobe type 1 neurons (TuLAL1 neurons), from the sky-compass pathway [18]. The AOTU consists of a large, spherical medial compartment (AOTUm) to which two smaller domains [intermediate AOTU (AOTUin) and lateral AOTU (AOTUl)] are attached [1] (Fig. 1A). In many other insects, the AOTU is oriented such that the larger domain is located dorsally of the smaller domains, and are therefore called the upper unit (AOTU-UU) and lower unit, or lower unit complex (AOTU-LU, AOTU-LUC), respectively. DALcl1d TuBu neurons appear to have

short, proximal processes in the lateral AOTU (AOTUI), and distal terminals in the superior and anterior BU (BUs; BUa; Fig. 1C, E). DALc12d TuBu neurons innervate complementary regions, connecting the intermediate domain of the AOTU (AOTUin) with the inferior BU (BUi; Fig. 1D, E). We did not identify neurons projecting directly from the large AOTUm compartment to the CX.

Visual interneurons of the medulla provide input to the AOTUI and AOTUin *via* a thick fiber bundle, the anterior optic tract (AOT). Gal4 driver lines reveal several discrete subpopulations of such medullo-tubercular (MeTu) neurons with proximal dendrites extending in medulla layer m6–8 (Fig. 1F, G) and distal axonal branches confined to the lateral and intermediate AOTU. Putative homologies between neurons of the AVP and the sky-compass pathway from other insects are summarized in Table 1.

By expressing reporter proteins specifically targeted to presynaptic terminals (*UAS-syt.GFP*) and postsynaptic membranes (*UAS-DenMark*) we can show that the anterior visual pathway is directed from the medulla to the anterior optic tubercle and, from there, towards the ellipsoid body. Thus, projections of DALv2 R neurons are mostly axonal in the EB, and dendritic in the BU (Fig. 1H). Likewise, projections of DALc11/2 TuBu neurons have mostly presynaptic, axonal sites in the bulb, and postsynaptic, dendritic sites in the AOTU (Fig. 1I). Proximal neurites of MeTu neurons in the medulla are exclusively dendritic; distal projections in the AOTU appear to possess intermingled presynaptic and postsynaptic sites (Fig. 1J). Although the AVP is predominantly centripetal, the presence of dendritic and axonal signal in the centrifugal direction suggests potential feedback in this circuit.

Ring neuron subclasses of DALv2 establish a topographically ordered connectivity between the bulb and ellipsoid body

Global markers for neuropil [antibodies against DN-cadherin (DNcad) or Bruchpilot (Brp)] in conjunction with specific Gal4 driver lines reveal more detail about the intricate anatomy and connectivity within the anterior visual pathway. In the EB, five discrete domains can be distinguished based on different expression levels of DN-cadherin (Fig. 2A–C). These comprise an inner posterior domain (EBip) and inner central domain (EBic) with low DNcad signal, an outer central domain (EBoc) with moderate DNcad signal, and an anterior domain (EBa) and outer posterior domain (EBop) with high signal. The bulb consists of three major domains defined by their position relative to the LEa fiber bundle formed by DALv2-derived ring (R) neuron axons. The superior and inferior domains of the bulb are located dorsally and ventrally of the LEa, respectively; the anterior bulb is attached to the lateral surface of the LEa at a position where it bends medially (Fig. 2A, B). DNcad labeling reveals the individual, large input synapses, called microglomeruli, formed by R neuron dendrites (Fig. 2B, arrowheads).

We screened the expression patterns of several Gal4 driver lines which label subpopulations of R neurons [30]. This analysis, in conjunction with single-cell labeling using the multicolor flip-out method (MCFO) [31], reveals that the ring domains of the ellipsoid body are connected in a topographically ordered pattern to the bulb, consistent with previous reports [32]. Previously unclassified R neurons innervating the anterior domain, which we call R5 (Fig. 2D–F), and R2 neurons of the outer central domain (Fig. 2G–I) have dendrites

in the superior bulb; other R neurons innervating the outer central domain are connected to the anterior bulb (R4m; Fig. 2J–L). R neurons innervating the inner central and inner posterior domain possess dendrites in the inferior bulb (R3; Fig. 2M–O).

We did not identify any ring neurons which form axons in the outer posterior domain of the ellipsoid body. This domain, as well as the other domains of the EB, is innervated by two main classes of columnar neurons that interconnect the different compartments of the central complex, PB-EB-gall (“wedge”) neurons (Fig. 2P, Q) and PB-EB-NO (“tile”) neurons (Fig. 2R) [33]. Both represent sublineages of four large type II lineages (DM1/DPMm1, DM2/DPMpm1, DM3/DPMpm2, DM4/CM4) [26,34], whose cell bodies are located in the posterior brain. Wedge neurons have proximal branches in the protocerebral bridge; from here they extend forward, through the fan-shaped body, into the EB where they presumably receive R neuron input. Collateral branches of wedge neurons project further forward into the gall of the lateral accessory lobe (LAL) [1,33] (Fig. 2P, Q); the LAL is a region thought to be relevant for locomotor output in insects [35]. Tile neurons have a more restricted projection to the outer posterior EB (Fig. 2R), and therefore overlap extensively with wedge neurons but not R neurons.

Tuberculo-bulbar neurons of DALcl1 and DALcl2 form a topographically ordered projection between the anterior optic tubercle and bulb

In view of the ordered connectivity between bulb and ellipsoid body, it stands to reason that neurons of DALcl1 and DALcl2, which connect the anterior optic tubercle to the bulb, are also topographically organized. Based on D_Ncad expression, three subdomains (medial, intermediate, lateral) can be defined for the AOTU [1]. Closer inspection of D_Ncad-labeled brains revealed that the intermediate domain is further subdivided into two narrow, vertical slices, named (from lateral to medial), AOTUil and AOTUim (Fig. 3A, B). The lateral domain, AOTUl, is divided into three finger-like processes (AOTUla, AOTUlc, AOTUlp) that are most easily revealed in horizontal sections of the tubercle (Fig. 3B).

We identified multiple Gal4 driver lines expressed in subpopulations of medullo-tubercular (MeTu) neurons and DALcl1 and 2-derived tuberculo-bulbar (TuBu) neurons whose projection is predominantly restricted to specific subdomains of the AOTU, additionally corroborated by MCFO-labeled single cell clones. The DALcl1-derived TuBu subpopulation with axons terminating primarily in the superior bulb (TuBu_s), has dendrites enriched in all three process of the lateral subdomain (AOTUla/c/p), and can be labeled by *R88A06-Gal4* (Fig. 3D–F). TuBu neurons terminating in the anterior bulb (TuBu_a), also derived from DALcl1, actually exhibit dendrites filling the lateral slice of the intermediate AOTU subdomain (AOTUil) (Fig. 3G–I). Dendrites of inferior bulb tuberculo-bulbar neurons (TuBu_i), derived from DALcl2, are concentrated in the medial intermediate subdomain (AOTUim) and express *R49E09-Gal4* (Fig. 3J–L). The parallel pathways connecting the anterior optic tubercle with the bulb and ellipsoid body are schematically summarized in Fig. 4.

MeTu neurons from the medulla (previously described [36] as medullar columnar 61 neurons; MC61) also terminate in specific subdomains of the lateral and intermediate AOTU defined by the dendrites of TuBu neurons. The AOTUm receives input from the lobula

(lobula columnar 10; LC10) [37]. Numerous driver lines expressed in MeTu neurons have been identified; three representative examples are depicted in Fig. 3M–T. Dendrites fill predominantly layer m7, with sparser branches reaching up into m6 (the layer contacted by photoreceptors R7) and deeper into m8. The somata of some MeTu neurons are distributed throughout the dorsal half of the medulla cortex, as shown here for neurons innervating the AOTUil domain (MeTu_{ij}; Fig. 3Q, R) and the AOTUim domain (MeTu_{im}; Fig. 3S, T). Cell bodies of other MeTu neurons, such as those innervating AOTUI (MeTu_j; Fig. 3M, N), are spread out over the entire medulla. Single cell clones of MeTu₁ (*R73C04-Gal4*) reveal that the dendritic tree arborizes locally of the primary neurite and covers 10–15 contiguous medulla columns (Fig. 3O–O’). Therefore, this class of neurons collectively innervates the entire medulla, rather than each individual neuron doing so, identifying MeTu neurons as special subclasses of multicolumnar medullary visual projection neurons. Their cell body location and projection pattern is reminiscent of *Drosophila* transmedullary neurons but, exhibit a single dendritic tree, and instead of targeting the lobula complex, directly project to the central brain [38].

Concomitant labeling of DALc11 or DALc12 TuBu neurons and DALv2 R neurons demonstrates that the endings of the former fully overlap with the proximal branches of the latter in the bulb (Fig. 4B, C). Given the large size of the pre- and postsynaptic endings, forming microglomeruli of approximately 2 μm diameter, it was evident that individual R neuron dendrites were directly contacted by TuBu neuron axons. To provide further evidence for a direct synaptic contact, we carried out a GRASP analysis, in which the post-synaptic cells are expressing CD2-RFP and split-GFP11, whereas the presynaptic cells express split-GFP1-10. As shown in Fig. 4D and E, a strong GRASP signal is detected specifically in the bulb within the expected target region. DALc11-derived TuBu_s neurons innervate R2 neurons of EBoc with microglomerular dendrites in the superior bulb, whereas DALc12-derived TuBu_i neurons innervate R3 neurons of EBic in the inferior bulb, confirming the presence of parallel, superior and inferior bulb pathways.

Lineally-organized input channels to the ellipsoid body form parallel neural ensembles that are functionally-distinct

Previous studies utilizing pan-neuronal or ring neuron-specific (R2 and R4d) two-photon calcium imaging in the superior bulb demonstrated that a subpopulation of R neuron dendrites respond to visual features. Visually-responsive dendritic microglomeruli typically exhibit ipsilateral receptive fields, bright (ON)-selectivity, and vertical orientation tuning [17]. Our anatomical data demonstrate that TuBu neurons provide direct input to R neuron dendrites; we therefore tested the hypothesis that the microglomerular presynaptic terminals of TuBu neurons exhibit similar physiological properties as R neuron dendrites. We expressed the genetically-encoded calcium indicator GCAMP6m under the control of *R88A06-Gal4*, which predominantly labels TuBu_s, the superior bulb-innervating neurons of DALc11 (Fig. 3D–F and 4B). Quiescent flies were placed in front of a curved visual display of LEDs and presented with different visual stimuli (Fig. 5A) while conducting two-photon calcium imaging from the microglomerular axonal outputs of these neurons (Fig. 5B). Recordings were conducted in two planes to maximally detect microglomerular activity (see Supplemental Experimental Procedures). Responsive superior bulb microglomeruli from

both planes exhibited qualitatively homogenous characteristics and were therefore analyzed collectively, in contrast to inferior bulb microglomeruli (see below).

Receptive field mapping with a small bright (ON) object revealed that TuBu_s outputs in the superior bulb each exhibit small, retinotopically-organized receptive fields that are localized to, and provide wide coverage of, the ipsilateral visual hemifield (Fig. 5C,D). The average receptive field size was 29.2° and 44.2° ($\pm 3.5^\circ$ and $\pm 2.8^\circ$ standard deviation, minor axis and major axis lengths respectively (Fig. 5E). The relative positioning of individual microglomeruli roughly corresponds to the positioning of the spatial receptive fields along the animal's visual elevation (Fig. 5F and G, top panels) and azimuth (Fig. 5F and G, bottom panels). In other words, microglomeruli with receptive fields located on the lower part of the visual field cluster in the ventrolateral part of the superior bulb, whereas microglomeruli located in the dorsomedial portion of the superior bulb have receptive fields located on the upper part of the visual field (Fig. 5F,G). Similarly, medially located microglomeruli tend to respond to visual stimulation on the medial portion of the ipsilateral visual field, whereas laterally located microglomeruli respond on the lateral portion of it (Fig. 5F,G). Spatial receptive fields of individual presynaptic microglomeruli were similar in size within and between animals (Fig. 5E).

As R neuron dendrites are tuned to vertically-oriented features, we next presented a horizontally moving bar spanning the full vertical extent of the display. Responses to a moving bright (ON) bar on a dark background much larger by comparison to OFF-bar response, indicating that TuBu_s neurons, like their downstream ring neurons, are ON-selective (Fig 5H) [17]. As a population, TuBu_s neurons respond maximally to a small ON object, slightly less to a bar and much less to a wide-field grating (Fig. 5I). These results might suggest that TuBu_s neurons respond to best to objects that fill the excitatory receptive field. Presentation of the ON object outside the excitatory receptive field did not generate measurable decreases in calcium accumulation (Fig. 5J), suggesting that surround inhibition is weak if present at all. Taken together, the response properties of TuBu_s neuron presynaptic terminals resemble those of superior bulb-associated ring neuron dendrites from previous reports [17], corroborating their role as direct presynaptic inputs.

We hypothesized that due to their distinct developmental origin, DALcl2-derived TuBu_i neurons, which innervate the inferior bulb, should exhibit functional dissimilarity to superior bulb innervating, DALcl1 TuBu_s neurons (Fig. 1C–E). Flies expressing GCAMP6m under the control of the predominantly TuBu_i neuron driver, *R49E09-Gal4*, were presented with the same battery of visual stimuli as shown for TuBu_s neuron microglomeruli. Unlike superior bulb TuBu_s neurons, responses in the inferior bulb TuBu_i neurons were heterogenous and variable (see Supplemental Experimental Procedures, Fig. S2); yet we identified one consistent response type for at least one microglomerulus in both imaging planes for every fly (Fig. 6A,C). The receptive fields scanned in the first imaging plane typically showed excitation to objects in the contralateral visual hemifield and inhibition when the object entered the ipsilateral visual hemifield (Fig. 6B, Fig. 6D mint green). TuBu_i microglomeruli showed peculiar secondary excitation as the object left the ipsilateral visual field at which time no visual stimulation was present (Fig. 6B black arrows, Fig. 6D mint green, black arrows). Qualitatively similar responses were observed from microglomeruli in

the second imaging plane (Fig. 6C), yet these responses were smaller in amplitude (Fig. 6D orange). In addition, we observed microglomerular structures that did not respond to any of our stimuli (Fig. 6C, microglomeruli that are not encircled orange).

TuBu_i responses were asymmetric with respect to stimulus motion direction. When an object moved from the ipsilateral visual hemifield towards the contralateral one, microglomeruli responded by slight excitation followed by inhibition (Fig. 6D'). We observed a strong response as the object entered the contralateral visual field (Fig. 6D'). Inferior bulb response characteristics were consistent across 104 microglomeruli in 15 flies (Fig. 6E and E') and they were distinct from superior bulb responses. In contrast to the superior bulb, the physiological responses of ring neurons that extend dendrites into the inferior bulb (R3) have not been systematically characterized, preventing us from making direct input-output comparisons. Nevertheless, the optophysiological analysis of separate TuBu neuron populations derived from DALc11 and DALc12 confirm the notion that different lineages form functionally-distinct neuronal ensembles.

In addition to the distinct temporal dynamics of inferior and superior bulb TuBu neuron object responses, we noted that the inferior bulb microglomeruli have larger spatial receptive fields that cover the entire contralateral visual hemifield and are very similar across microglomeruli, showing strongest responses to visual stimuli presented on the upper portion of the display (Fig. 6B) or after the stimulus left the screen. Whereas the spatial receptive fields and temporal response properties are distinct between superior bulb and inferior bulb, the preference for ON objects is similar (Fig. 6F). Also, like superior bulb TuBu_s neurons, the inferior bulb TuBu_i neurons respond very weakly to wide-field gratings by comparison to small objects or bars (Fig. 6G, see above). Our results indicate that both superior and inferior bulb-innervating TuBu neurons are sensitive to bright objects but sample unique hemifields; ipsilateral and contralateral fields, respectively, with distinct receptive field structure and temporal dynamics.

Discussion

The anterior visual pathway (AVP) described in this work serves to define the architecture of a circuit that projects from peripheral neuronal elements of the medulla to the EB neurons of the *Drosophila* CX sequentially *via* medullo-tubercular (MeTu) neurons, and parallel superior DALc11 and inferior DALc12 pathways (TuBu_s and TuBu_i neurons). The CX plays a pivotal role in innate and learned visually-guided behaviors. Recent studies by Seelig and Jayaraman [10,17] examined the physiological responses of neuronal subpopulations within the EB. They first observed that individual R neurons whose dendritic microglomeruli are localized in the superior bulb (R2 and R4d), respond to visual stimuli. Here, we identify the developmentally-related TuBu_s neurons of DALc11 as the direct pre-synaptic inputs to these superior bulb R neurons, and demonstrate that many of their visual tuning properties can already be observed in the upstream TuBu_s population (Fig 5). In addition, we identify DALc12-derived TuBu_i neurons, which exhibits distinct receptive field properties from TuBu_s neurons (Fig 6), and likely supply the inferior bulb R neurons (presumably R3 neurons of the EBic domain) that have not been systematically characterized previously. TuBu_i neurons' unique receptive field and response properties suggest input from

contralaterally located neurons. Indeed, neurons innervating the anterior optic tubercle on both sides, described in other insects, may account for the visual interhemispheric receptive field characteristics described here and in other neurons of the sky-compass pathway [39,41,50].

R neurons, whose axons cover the entire perimeter of the ellipsoid body, provide input to the large number of columnar neurons (so called “wedge neurons”; [33]), the neurites of which subdivide the torus-shaped volume of the ellipsoid body into narrow radial partitions. The calcium dynamics recorded from the population of wedge neurons produces a localized “bump” of activity in the torus which, based on visual landmarks and proprioception, corresponds to an internal representation of the animal’s orientation in space [10]. Information likely reverberates between the EB and other CX neuropils, such as the protocerebral bridge, *via* different populations of columnar elements (wedge and tile neurons) which heavily interconnect them [33]. Similarly to the head direction system in mammalian brains, these dynamics produce stable neural activity consistent with an internal compass [10]. The EB displays a common organizational principle observed in complex nervous systems; in essence, it is a structure arranged into layers and columns by tangential (ring neurons) and columnar (wedge and tile neurons) elements, respectively. A receptive field-specific response in a single R neuron would presumably influence activity in an entire layer, and thus all columns. One of the most insightful lines of inquiry will be to investigate how this tangential input is translated into (or is even compatible with) the localized columnar activity (“bump”) within the wedge neurons of the EB. It is conceivable that R neurons, due to their peculiar bifurcated architecture, may influence EB wedges with a physiologically-relevant temporal offset, which could be utilized to modulate spatially-restricted activity patterns. Future work defining the circuit motifs present in this brain region may provide insight into the advantages of a layered and columnar organization for emergent neural properties, such as a cognitive-like internal representation and navigation.

The neurons and neuropil compartments of the *Drosophila* AVP have homologous counterparts in other insects, forming the so-called “sky-compass pathway”, most prominently investigated in the locust, (*Schistocerca gregaria*; [18,39,40]), monarch butterfly (*Danaus plexippus*; [42]), honeybee (*Apis mellifera*; [22]) and bumblebee (*Bombus ignitus*; [21]). MeTu neurons providing input to the AVP form dendritic branches within the boundary region of distal and proximal medulla [21,22,43]. The target neuropil innervated by MeTu neurons is the lateral/intermediate part of the AOTU, called the “lower unit or lower unit complex” of the AOTU (AOTU-LU or LUC) in locust and other insects [1,39,44]. Two classes of neurons, TuLAL1a and TuLAL1b, likely counterparts of the TuBu neurons described in this paper, form two parallel pathways that convey the output from the AOTU-LUC to small neuropil foci within the LAL which are homologous to the bulb, formerly called the lateral triangle and median olive. From here, TL neurons, homologs of fly R neurons, carry the visual input to the lower unit of the central body, counterpart of the *Drosophila* ellipsoid body [18]. Based on the available anatomical and functional data, it is not yet possible to propose more specific homologies between neuron classes of the AVP in flies, and the corresponding sky compass pathway in other insects.

Most notably recognized as the polarization (POL) vision pathway, neurons of the sky-compass network are tuned to the e-vectors of polarized light which reflect the location of the sun, thus providing compass information used by these insects to navigate during long range migrations or local path integration in central place foraging [42,45]. Considering that *Drosophila* also exhibits physiological and behavioral correlates with POL sensitivity [46–48], we posit that the fly AVP is the neural circuit for POL information transmission to the CX. However, a recent report demonstrated that when flies are presented with a rotating field of polarized UV light in conjunction with pan-neuronal calcium imaging, robust calcium signals in any CX neuropils, including the bulb, were not observed [49]. In contrast, and in agreement with our findings, bright objects elicited strong responses in the bulb and other regions of the CX. Indeed, neurons of the sky-compass pathway can encode both a specific e-vector and the azimuthal position of an unpolarized light source, the nature and degree of which depends on the insect and neuron type in question [24,40,42,50]. The extent of encoding strength to a given stimulus (polarized versus unpolarized light) likely reflects the ethology and ecological niche of the animal. For example, diurnal dung beetles utilize the position of a bright object (such as the sun or moon) to navigate regardless of ambient light intensity, whereas nocturnal beetles utilize polarized skylight specifically at low light intensities, rather than position of a celestial body such as the moon. This ethological distinction is reflected in the tuning properties of neurons within the sky-compass pathway, even between two closely-related insects [24].

In the *Drosophila* AVP, the spatial position of luminance cues emanating from a bright source, such as a celestial body or an escape route from within foliage, would be represented more strongly than the skylight pattern of polarized light [49]. This proposition is based on the following:

1. Anatomical and ethological evidence: In comparison to other insects examined, in which an aspect of their behavioral repertoire is thought to depend on POL vision, the ethological lifestyle of *Drosophila* suggests that it may be less likely to use the pattern of polarized skylight to navigate. This fact is reflected in their relatively rudimentary dorsal rim area (DRA), a region of the eye with specialized, POL-sensitive photoreceptors, and correspondingly inconspicuous dorsal rim area of the medulla (MEDRA), which receives input from DRA photoreceptors. In addition, likely homologues of MeTu neurons in other insects (transmedulla neurons) often exhibit long, dorsally-projecting input neurites which ramify in the MEDRA, suggesting a high degree of POL input [21,22]. In contrast, we did not observe this characteristic feature in MeTu neurons in *Drosophila*; dendritic arborizations ramified locally of the primary neurite, which were distributed relatively evenly throughout the dorsal half of, or the whole eye.
2. Upstream TuBu as well as downstream R neurons and wedge neurons show strong excitation to bright objects [10,17], whereas dark object responses are weaker (Figs. 5 and 6), suggesting specialization for detecting a bright object against a dark background. The ON-preference and weak tuning to object size by TuBu neurons (Figs. 5 and 6) suggest that this pathway would poorly mediate stripe fixation behavior, which is activated more by dark bars or complex motion-

defined edges [51]. However, the topographical organization of TuBu_s neuron terminals (Fig. 5) suggests that retinotopy is conserved and thus could serve spatial navigation, unlike other small-object visual projection neurons (VPNs) of the lobula and lobula plate where the retinotopy is apparently lost within the intermingled axon terminals of individual small-field columnar neurons [52,53].

3. The preference for bright objects of varying size suggests that the CX receives rather primitive spatial information by comparison to the complex filtering properties exhibited by other VPN pathways that act as precise spatial filters for directional patterns of optic flow, the spatial dynamics of looming objects, and the omni-directional motion of small OFF-contrasting objects [52–54].
4. Spatial interactions of excitation and inhibition: A single bright object presented ipsilaterally against a dark background would excite a spatially defined subset of ipsilateral TuBu_s neurons while simultaneously exciting multiple (possibly all) canonical contralateral TuBu_i neurons. By contrast, two bright spots appearing in the left and right visual fields would simultaneously stimulate TuBu_s neurons on both right and left side while leading to inhibition in all TuBu_i neurons. Most intriguingly, TuBu_i neurons show strong calcium currents as a bright object leaves the visual field suggesting that TuBu_i neurons might be signaling to the R neurons some crucial information about ‘losing’ the visual bearing to a bright object. R neurons have shown to be indispensable for visual place learning [8] and it is possible that inferior bulb neurons have a crucial role in carrying some of the visual information that is used by R neurons to mediate this behavior.

Here we provide ample evidence that DALc1 and DALc2-derived neurons have unique functional properties, come from distinct lineages, and supply visual information to the central complex. To our knowledge, this is the first extensive characterization of the visual input to the central complex in *Drosophila*, and a definitive example of how developmentally distinct lineages give rise to functionally distinct circuits.

Experimental Procedures

Drosophila stocks

Flies were reared at 25°C using standard fly media unless otherwise noted. The *Drosophila* driver lines utilized in this study, as well as more specific genotype information, are listed in the Supplemental Experimental Procedures. The following general transgenic fly stocks were used: *UAS-DenMark::mCherry*, *UAS-Syt::GFP*, *su(Hw)attP8:HA_V5_FLAG_1* [31], *10xUAS-mCD8::GFP*, *10XUAS-IVS-mCD8::RFP*, *13XLexAop2-mCD8::GFP*, *LexAop-CD2::RFP*, *UAS-CD4::spGFP1-10*, *LexAop-CD4::spGFP11*, *20xUAS-GCAMP6m* (Bloomington Stock Center, Bloomington, Indiana).

Clonal analysis

GFP-labeled adult neuroblast MARCM clones were induced at the late first instar/early second instar stage by heat-shocking in a water bath at 38 °C for 30–60 min. Larvae were approximately 12–44 hours old. Heat-shocked larvae were grown to adult for analysis.

Single cell analysis of neurons in the AVP pathway was conducted using the multicolor flip-out (MCFO) method described previously [31,33]. Briefly, depending on the cell density of a given Gal4 line, 1–3 day old flies were dissected to obtain single cell labeling.

Immunostaining, confocal microscopy, and image analysis

Immunohistochemistry was performed using standard procedures with some modifications [26], details for staining procedures and list of antibodies are in Supplemental Experimental Procedures. *Drosophila* adult brains labeled with antibody markers were viewed as whole-mounts in Vectashield mounting medium H-1000 (Vector Laboratories), by confocal microscopy [LSM 700 Imager M2 using Zen 2009 (Carl Zeiss Inc.); lenses: 40× oil (numerical aperture 1.3)]. Complete series of optical sections were taken from preparations between 1.2 and 2- μ M intervals. Preparations were mounted anteriorly or dorsally. Dorsally-oriented preparations were acquired by sliding the brain dorsal-side up, inside the crevice between two closely apposed cover slips. Captured images were processed by ImageJ or FIJI (National Institutes of Health, <http://rsbweb.nih.gov/ij/> and <http://fiji.sc/>). In Fig. 1B–G, background labeling was manually removed to improve clarity of specific neuronal morphologies. In Fig. 1E, ventral hemilineages of DALc1/2 were digitally removed, and z-projections of the labeled dorsal hemilineages were registered digitally with z-projections of a standard brain at the corresponding antero-posterior plane using the scaling and warping tool in the NIH ImageJ and Adobe Photoshop software programs. Easily recognizable landmarks, including the center of the peduncle and ellipsoid body, and the tips of the mushroom body lobes were used as fiduciary points. For multicolor flip-out experiments, additional non-overlapping neurons were manually removed, and anti-Brp labeled neuropil compartments were outlined with hatched lines from the same sample. Schematics were made in Adobe Illustrator and figures assembled in Adobe Photoshop.

Two-photon calcium imaging, visual stimuli, and two-photon imaging analysis

Calcium imaging was conducted as previously described [53]. Briefly, calcium-dependent fluorescent signals were detected using a two-photon excitation scanning microscope (3i, Boulder, CO) with Slidebook 6 software (3i, CO), at an image acquisition rate of 10 frames/sec. 3–7 day old female flies expressing *20xUAS-GCAMP6m* under the control of a specific Gal4 driver labeling tuberculo-bulbar neuron subpopulations were used; all recordings were conducted from the microglomerular presynaptic terminals of these neurons. Flies were immobilized in a custom holder and bathed in physiological saline; neurons of interest were made optically accessible by dissecting the posterior cuticle of the head capsule. Visual stimuli were presented to the fly using a 96×32 pixel LED arena. Specific details of two-photon imaging setup, visual stimuli, and imaging analysis are provided in Supplemental Experimental Procedures.

Supplementary Material

Refer to Web version on PubMed Central for supplementary material.

Acknowledgments

We thank Orkun Akin for kindly sharing the image alignment algorithm. We also thank Hiroshi Shiozaki and Hokto Kazama for discussing unpublished results. This work was supported by the National Institutes of Health (R01 NS096290 to V.H., and R01 EY026031 to M.A.F.), the Ruth L. Kirschstein National Research Service Award (J.J.O, No. GM007185), the UCLA Edith Hyde Fellowship (M.F.K), and the University of California, Los Angeles Dissertation Year Fellowship (J.J.O and M.F.K).

References

1. Ito K, Shinomiya K, Ito M, Armstrong JD, Boyan G, Hartenstein V, Harzsch S, Heisenberg M, Homberg U, Jenett A, et al. A systematic nomenclature for the insect brain. *Neuron*. 2014; 81:755–765. [PubMed: 24559671]
2. Strausfeld NJ. *Atlas of an Insect Brain*. Springer. 1976; 52:1096–1109.
3. Hanesch U, Fischbach KF, Heisenberg M. Neuronal architecture of the central complex in *Drosophila melanogaster*. *Cell Tissue Res*. 1989; 257:343–366.
4. Huber F. Untersuchungen über die Funktion des Zentralnervensystems und insbesondere des Gehirnes bei der Fortbewegung und der Lauterzeugung der Grillen. *Zeitschrift für Vergleichende Physiol*. 1960; 44:60–132.
5. Otto D. Untersuchungen zur zentralnervösen Kontrolle der Lauterzeugung von Grillen. *Zeitschrift für Vergleichende Physiol*. 1971; 74:227–271.
6. Strauss R, Heisenberg M. A higher control center of locomotor behavior in the *Drosophila* brain. *J Neurosci*. 1993; 13:1852–61. [PubMed: 8478679]
7. Ilius M, Wolf R, Heisenberg M. The central complex of *Drosophila melanogaster* is involved in flight control: studies on mutants and mosaics of the gene *ellipsoid body open*. *J Neurogenet*. 2007; 21:321–38. [PubMed: 18161592]
8. Ofstad TA, Zuker CS, Reiser MB. Visual place learning in *Drosophila melanogaster*. *Nature*. 2011; 474:204–207. [PubMed: 21654803]
9. Neuser K, Triphan T, Mronz M, Poeck B, Strauss R. Analysis of a spatial orientation memory in *Drosophila*. *Nature*. 2008; 453:1244–1247. [PubMed: 18509336]
10. Seelig JD, Jayaraman V. Neural dynamics for landmark orientation and angular path integration. *Nature*. 2015; 521:186–191. [PubMed: 25971509]
11. Poucet B, Chaillan F, Truchet B, Save E, Sargolini F, Hok V. Is there a pilot in the brain? Contribution of the self-positioning system to spatial navigation. *Front Behav Neurosci*. 2015; 9:292. [PubMed: 26578920]
12. Lai SL, Awasaki T, Ito K, Lee T. Clonal analysis of *Drosophila* antennal lobe neurons: diverse neuronal architectures in the lateral neuroblast lineage. *Development*. 2008; 135:2883–93. [PubMed: 18653555]
13. Das A, Gupta T, Davla S, Prieto-Godino LL, Diegelmann S, Reddy OV, Raghavan KV, Reichert H, Lovick J, Hartenstein V. Neuroblast lineage-specific origin of the neurons of the *Drosophila* larval olfactory system. *Dev Biol*. 2013; 373:322–37. [PubMed: 23149077]
14. Hartenstein, V., Spindler, S., Peraanu, W., Fung, S. *Brain Development in Drosophila melanogaster*. New York, NY: Springer New York; 2008. *The Development of the Drosophila Larval Brain*; p. 1-31.
15. Jefferis GSXE, Marin EC, Stocker RF, Luo L. Target neuron prespecification in the olfactory map of *Drosophila*. *Nature*. 2001; 414:204–208. [PubMed: 11719930]
16. Marin EC, Jefferis GSXE, Komiyama T, Zhu H, Luo L. Representation of the glomerular olfactory map in the *Drosophila* brain. *Cell*. 2002; 109:243–55. [PubMed: 12007410]
17. Seelig JD, Jayaraman V. Feature detection and orientation tuning in the *Drosophila* central complex. *Nature*. 2013; 503:262–266. [PubMed: 24107996]
18. el Jundi B, Pfeiffer K, Heinze S, Homberg U. Integration of polarization and chromatic cues in the insect sky compass. *J Comp Physiol A*. 2014; 200:575–589.

19. Träger U, Wagner R, Bausenwein B, Homberg U. A novel type of microglomerular synaptic complex in the polarization vision pathway of the locust brain. *J Comp Neurol.* 2008; 506:288–300. [PubMed: 18022957]
20. Heinze S, Florman J, Asokaraj S, el Jundi B, Reppert SM. Anatomical basis of sun compass navigation II: The neuronal composition of the central complex of the monarch butterfly. *J Comp Neurol.* 2013; 521:267–298. [PubMed: 22886450]
21. Pfeiffer K, Kinoshita M. Segregation of visual inputs from different regions of the compound eye in two parallel pathways through the anterior optic tubercle of the bumblebee (*Bombus ignitus*). *J Comp Neurol.* 2012; 520:212–229. [PubMed: 21953619]
22. Zeller M, Held M, Bender J, Berz A, Heinloth T, Hellfritz T, Pfeiffer K. Transmedulla neurons in the sky compass network of the honeybee (*Apis mellifera*) are a possible site of circadian input. *PLoS One.* 2015; 10:e0143244. [PubMed: 26630286]
23. Held M, Berz A, Hensgen R, Muenz TS, Scholl C, Rössler W, Homberg U, Pfeiffer K. Microglomerular synaptic complexes in the sky-compass network of the honeybee connect parallel pathways from the anterior optic tubercle to the central complex. *Front Behav Neurosci.* 2016; 10:186. [PubMed: 27774056]
24. el Jundi B, Warrant EJ, Byrne MJ, Khaldy L, Baird E, Smolka J, Dacke M. Neural coding underlying the cue preference for celestial orientation. *Proc Natl Acad Sci U S A.* 2015; 112:11395–400. [PubMed: 26305929]
25. Lovick JK, Ngo KT, Omoto JJ, Wong DC, Nguyen JD, Hartenstein V. Postembryonic lineages of the *Drosophila* brain: I. Development of the lineage-associated fiber tracts. *Dev Biol.* 2013; 384:228–257. [PubMed: 23880429]
26. Wong DC, Lovick JK, Ngo KT, Borisuthirattana W, Omoto JJ, Hartenstein V. Postembryonic lineages of the *Drosophila* brain: II. Identification of lineage projection patterns based on MARCM clones. *Dev Biol.* 2013; 384:258–89. [PubMed: 23872236]
27. Ito M, Masuda N, Shinomiya K, Endo K, Ito K. Systematic Analysis of Neural Projections Reveals Clonal Composition of the *Drosophila* Brain. *Curr Biol.* 2013; 23:644–655. [PubMed: 23541729]
28. Yu HH, Awasaki T, Schroeder MD, Long F, Yang JS, He Y, Ding P, Kao JC, Wu GYY, Peng H, et al. Clonal development and organization of the adult *Drosophila* central brain. *Curr Biol.* 2013; 23:633–643. [PubMed: 23541733]
29. Peraanu W, Kumar A, Jennett A, Reichert H, Hartenstein V. Development-based compartmentalization of the *Drosophila* central brain. *J Comp Neurol.* 2010; 518:2996–3023. [PubMed: 20533357]
30. Jenett A, Rubin GM, Ngo TTB, Shepherd D, Murphy C, Dionne H, Pfeiffer BD, Cavallaro A, Hall D, Jeter J, et al. A GAL4-Driver Line Resource for *Drosophila* Neurobiology. *Cell Rep.* 2012; 2:991–1001. [PubMed: 23063364]
31. Nern A, Pfeiffer BD, Rubin GM. Optimized tools for multicolor stochastic labeling reveal diverse stereotyped cell arrangements in the fly visual system. *Proc Natl Acad Sci.* 2015; 112:201506763.
32. Renn SC, Armstrong JD, Yang M, Wang Z, An X, Kaiser K, Taghert PH. Genetic analysis of the *Drosophila* ellipsoid body neuropil: organization and development of the central complex. *J Neurobiol.* 1999; 41:189–207. [PubMed: 10512977]
33. Wolff T, Iyer NA, Rubin GM. Neuroarchitecture and neuroanatomy of the *Drosophila* central complex: A GAL4-based dissection of protocerebral bridge neurons and circuits. *J Comp Neurol.* 2015; 523:997–1037. [PubMed: 25380328]
34. Yang JS, Awasaki T, Yu HH, He Y, Ding P, Kao JC, Lee T. Diverse neuronal lineages make stereotyped contributions to the *Drosophila* locomotor control center, the central complex. *J Comp Neurol.* 2013; 521:2645–2662. [PubMed: 23696496]
35. Namiki S, Kanzaki R. Comparative neuroanatomy of the lateral accessory lobe in the insect brain. *Front Physiol.* 2016; 7:244. [PubMed: 27445837]
36. Otsuna H, Shinomiya K, Ito K. Parallel neural pathways in higher visual centers of the *Drosophila* brain that mediate wavelength-specific behavior. *Front Neural Circuits.* 2014; 8:8. [PubMed: 24574974]

37. Panser K, Tirian L, Schulze F, Villalba S, Jefferis GSXE, Bühler K, Straw AD. Automatic Segmentation of *Drosophila* Neural Compartments Using GAL4 Expression Data Reveals Novel Visual Pathways. *Curr Biol.* 2016; 26:1943–1954. [PubMed: 27426516]
38. Fischbach KF, Dittrich aP. The optic lobe of *Drosophila melanogaster*. I: A Golgi analysis of wild-type structure. *Cell Tissue Res.* 1989; 258:441–475.
39. Homberg U, Hofer S, Pfeiffer K, Gebhardt S. Organization and neural connections of the anterior optic tubercle in the brain of the locust, *Schistocerca gregaria*. *J Comp Neurol.* 2003; 462:415–430. [PubMed: 12811810]
40. Pfeiffer K, Kinoshita M, Homberg U. Polarization-sensitive and light-sensitive neurons in two parallel pathways passing through the anterior optic tubercle in the locust brain. *J Neurophysiol.* 2005; 94:3903–3915. [PubMed: 16049147]
41. Heinze S, Gotthardt S, Homberg U, Biologie F. Transformation of Polarized Light Information in the Central Complex of the Locust. *J Neurosci.* 2009; 29:11783–11793. [PubMed: 19776265]
42. Heinze S, Reppert SM. Sun compass integration of skylight cues in migratory monarch butterflies. *Neuron.* 2011; 69:345–358. [Accessed January 17, 2017] [PubMed: 21262471]
43. el Jundi B, Pfeiffer K, Homberg U. A distinct layer of the medulla integrates Sky compass signals in the brain of an insect. *PLoS One.* 2011; 6:e27855. [PubMed: 22114712]
44. Heinze S, Reppert SM. Anatomical basis of sun compass navigation I: The general layout of the monarch butterfly brain. *J Comp Neurol.* 2012; 520:1599–1628. [PubMed: 22473804]
45. Homberg U, Heinze S, Pfeiffer K, Kinoshita M, el Jundi B. Central neural coding of sky polarization in insects. *Philos Trans R Soc Lond B Biol Sci.* 2011; 366:680–7. [PubMed: 21282171]
46. Weir PT, Dickinson MH. Flying *drosophila* orient to sky polarization. *Curr Biol.* 2012; 22:21–27. [PubMed: 22177905]
47. Wernet MF, Velez MM, Clark DA, Baumann-Klausener F, Brown JR, Klovstad M, Labhart T, Clandinin TR. Genetic dissection reveals two separate retinal substrates for polarization vision in *drosophila*. *Curr Biol.* 2012; 22:12–20. [PubMed: 22177904]
48. Weir PT, Henze MJ, Bleul C, Baumann-Klausener F, Labhart T, Dickinson MH. Anatomical Reconstruction and Functional Imaging Reveal an Ordered Array of Skylight Polarization Detectors in *Drosophila*. *J Neurosci.* 2016; 36:5397–5404. [PubMed: 27170135]
49. Weir PT, Dickinson MH. Functional divisions for visual processing in the central brain of flying *Drosophila*. *Proc Natl Acad Sci U S A.* 2015; 112:E5523–32. [PubMed: 26324910]
50. Pfeiffer K, Homberg U. Coding of Azimuthal Directions via Time-Compensated Combination of Celestial Compass Cues. *Curr Biol.* 2007; 17:960–965. [PubMed: 17524646]
51. Maimon G, Straw AD, Dickinson MH. A Simple Vision-Based Algorithm for Decision Making in Flying *Drosophila*. *Curr Biol.* 2008; 18:464–470. [PubMed: 18342508]
52. Wu M, Nern A, Williamson WR, Morimoto MM, Reiser MB, Card GM, Rubin GM. Visual projection neurons in the *Drosophila* lobula link feature detection to distinct behavioral programs. *Elife.* 2016;5.
53. Kele MF, Frye MA. Object-Detecting Neurons in *Drosophila*. *Curr Biol.* 2017 in press.
54. Maisak MS, Haag J, Ammer G, Serbe E, Meier M, Leonhardt A, Schilling T, Bahl A, Rubin GM, Nern A, et al. A directional tuning map of *Drosophila* elementary motion detectors. *Nature.* 2013; 500:212–6. [PubMed: 23925246]

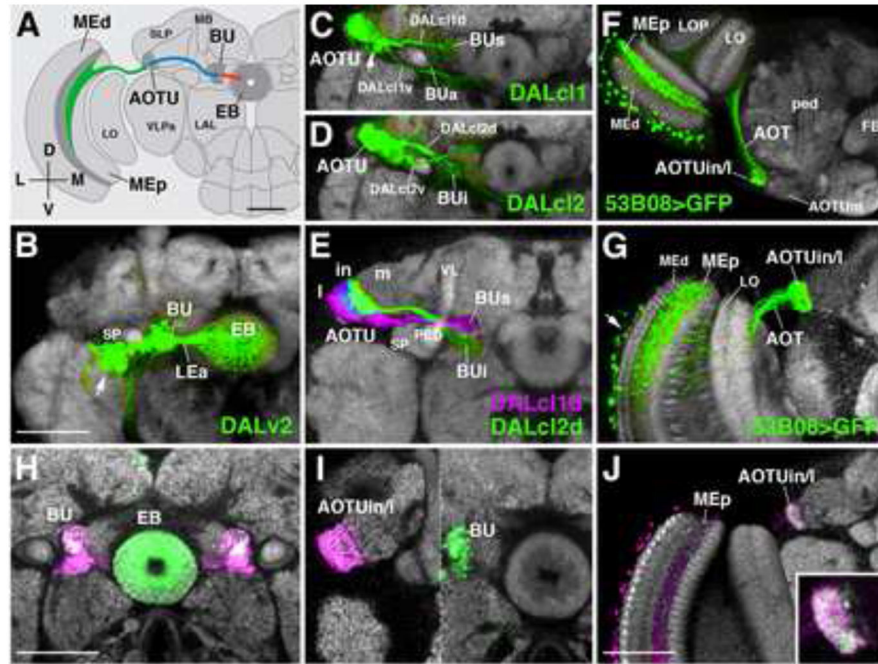


Figure 1. Discrete lineages constitute the central brain components of the anterior visual pathway

(B–J) Confocal z-projections illustrating the anterior visual pathway (AVP) (frontal sections unless otherwise noted); adult brains labeled with anti-DN-cadherin (grey), cell body clusters depicted by arrows.

(A) Schematized overview of the three-legged AVP. First leg (green): from the optic lobe medulla to the anterior optic tubercle (AOTU). Second leg (blue): from the AOTU to bulb (BU). Final leg (red): from the bulb (BU) to the ellipsoid body (EB) of the central complex.

(B–D) Mosaic analysis with a repressible cell marker (MARCM) clones of secondary lineages DALv2, DALc11, and DALc12 (green) (Nomenclature from [26,29]). (B) DALv2 forms all ring neurons of the EB (red leg in A), projecting from the BU to the EB *via* the anterior lateral ellipsoid body tract (LEa). (C and D) DALc11 and DALc12 form tuberculo-bulbar neurons (blue leg in A). Two tract components emanate from each neuroblast clone, a dorsal (DALc11/2d) and a ventral (DALc11/2v) component which we conclude are hemilineages. The dorsal, not ventral, hemilineages form the tuberculo-bulbar neurons.

(E) Isolation and registration of DALc11/2 dorsal hemilineages (see experimental procedures) (DALc11d; magenta, DALc12d; green). Neurites of DALc11d projects from the lateral domain of the AOTU (AOTU_l) to the superior domain of the bulb (BU_s), DALc12d projects from the intermediate domain of the AOTU (AOTU_{in}) to the inferior domain of the bulb (BU_i). We did not identify neurons projecting from the large medial domain of the AOTU (AOTU_m) to the bulb.

(F–G) Horizontal (F) and frontal (G) sections of *R53B05-Gal4* (green) labeling medullo-tubercular neurons, projecting from the medulla to the AOTU_{in/1} *via* the anterior optic tract (AOT) (green leg in A).

(H–J) Expression of pre-synaptic marker *syt::GFP* (green) and dendritic marker DenMark (magenta) in distinct legs of the AVP. (H) *R20A02-Gal4* labels most ring neurons and shows

enrichment of axonal output in the EB and dendrites in the BU. (I) *R48B06-Gal4* labels tuberculo-bulbar neurons and shows enrichment of output in the BU and dendrites in the AOTUin/1. (J) *R53B05-Gal4* demonstrates medullo-tubercular neurons are dendritic in the proximal medulla (MEp) but appears to have mixed dendritic and axonal specializations in the AOTUin/1 (boxed inset).

Other abbreviations: LAL, lateral accessory lobe; LO, lobula; LOP, lobula plate; MB, mushroom body; ME_d, distal medulla; PED, peduncle of the mushroom body; SP, spur of the mushroom body; SLP, superior lateral protocerebrum; VL, vertical lobe; VL_{Pa}, anterior ventrolateral protocerebrum

Scale Bars: 50µm (A, C, D, F); 50µm (B, E, G, J); 50µm (H, I)

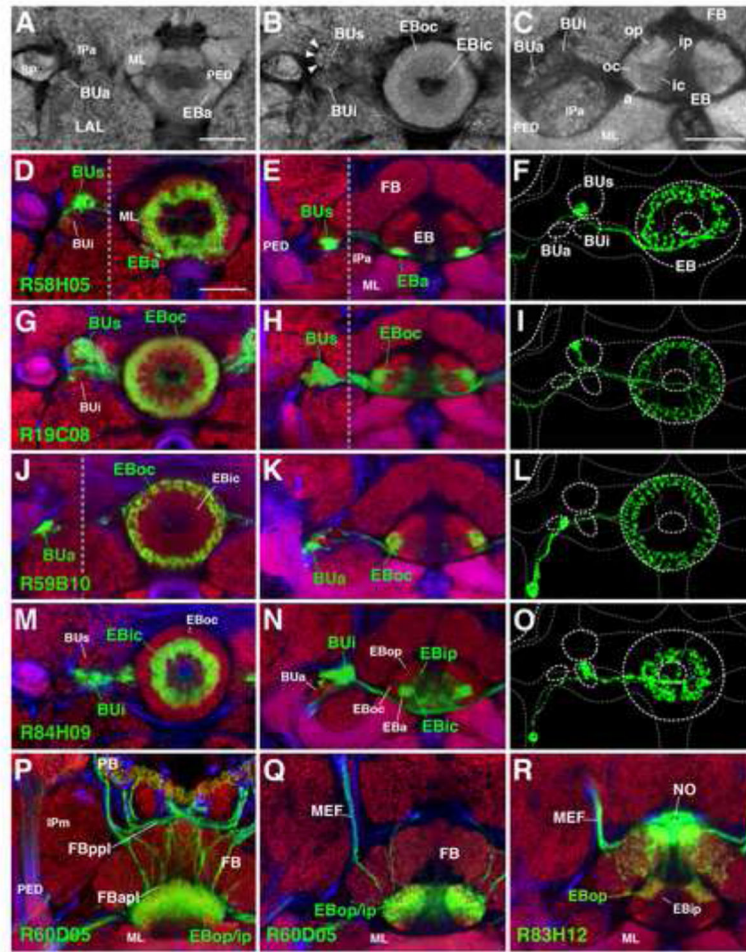


Figure 2. DN-Cadherin domains and single cell labeling define the topology and architecture of ellipsoid body neurons

(A–C) High magnification frontal (A and B) and horizontal (C) z-projections of the bulb and ellipsoid body neuropil labeled by anti-DN-cadherin (grey) reveals three distinct domains in the bulb and five distinct domains in the ellipsoid body. (A) Anterior frontal section reveals the anterior bulb (BUa) and the anterior domain of the EB (EBa). (B) Intermediate frontal section; reveals the superior (BUs) and inferior (BUi) domains of the bulb, and the outer central (EBoc) and inner central (EBic) domains of the EB. Arrowheads designate bulb microglomeruli. (C) Horizontal section through the EB canal reveals all five EB domains. (D–O) Gal4 drivers which label distinct ring neuron subclasses defined by axon morphology, and topology within the BU and EB. Each row represents a distinct Gal4 driver; first and second columns are frontal and horizontal sections labeled with *10xUAS-mCD8::GFP*, respectively, grey hatched lines denote regions of interest that are not within the same plane. Neuropil labeled with anti-DN-cadherin (red) and axon tracts by anti-Neuroglian (blue). Third column is a single cell clone generated by MCFO using the same Gal4 (see Experimental Procedures); white hatched lines outline neuropil compartments from the same fly. (D–F) *R58H05-Gal4* (R5; BUs to EBa). (G–I) *R19C08-Gal4* (R2; BUs to EBoc). (J–L) *R59B10-Gal4* (R4m; BUa to EBoc). (M–P) *R84H09-Gal4* (R3; BUi to EBic/ip). (P–R) *R60D05* (R3; BUi to EBic/ip). (R) *R83H12* (R3; BUi to EBic/ip).

(P–R) Horizontal confocal z-projections of Gal4 drivers labeling columnar elements. (P–Q) *R60D05-Gal4* labels PB-EB-gall (“wedge”) neurons. (P) Z-projection depicting the complete projection pattern of the population in the CX. (Q) Section through the EB canal; “wedge” neurons most densely occupy posterior EB domains, but diffusely project into intermediate and anterior domains as well. (R) *R83H12-Gal4* labels PB-EB-NO (“tile”) neurons, which fill the outer posterior domain of the EB (EBop).

Other abbreviations: FB, fan shaped body; FBapl and FBppl, anterior and posterior plexus of the fan shaped body; IPa and IPm, anterior and medial inferior protocerebrum; LAL, lateral accessory lobe; MEF, medial equatorial fascicle; ML, medial lobe of the mushroom body; NO, noduli; PB; protocerebral bridge; PED, peduncle of the mushroom body; SMP, superior medial protocerebrum; SP, spur of the mushroom body; VL, vertical lobe

Scale Bars: 25µm (A, B); 25µm (C); 25µm (D–R)

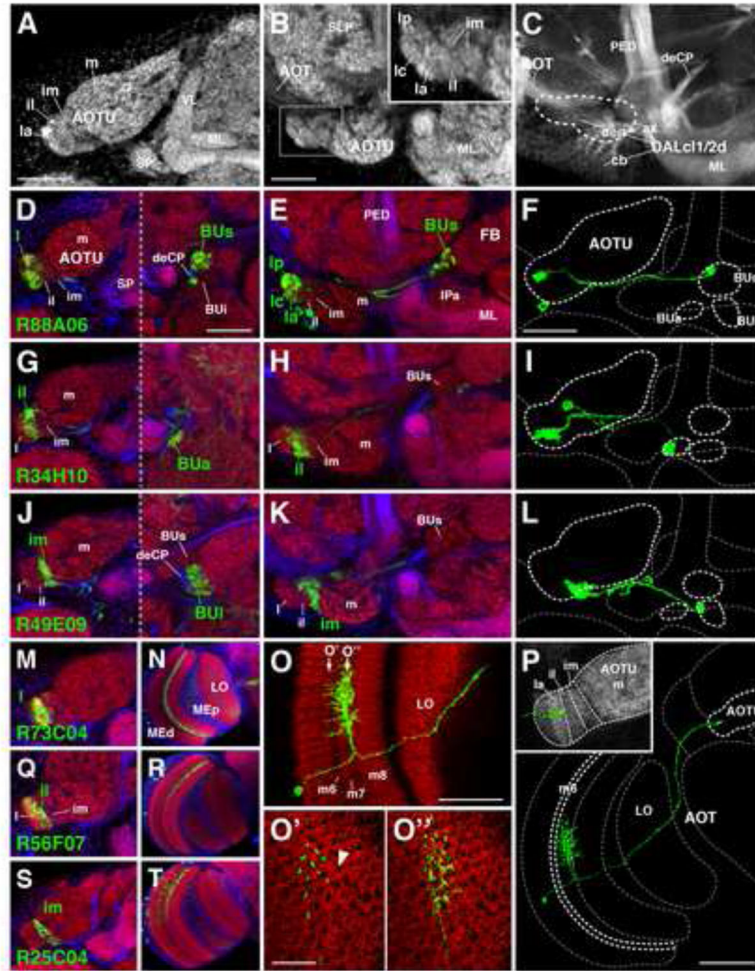


Figure 3. Topology and architecture of tuberculo-bulbar and medullo-tubercular neurons
 (A–C) High magnification frontal (A) and horizontal (B and C) z-projections of the anterior optic tubercle reveals six distinct domains in the AOTU (m, medial; im, intermediate medial; il, intermediate lateral; la/c/p, lateral anterior/central/posterior), highlighted by boxed inset in (B). Neuropil labeled by anti-DN-cadherin (grey; A and B), axon tracts labeled by anti-Neuroglial (grey; C) with AOTU location denoted by white hatched line with locations of DALc11/2d cell bodies (cb), dendrites (den), and axons (ax).

(D–L) Gal4 drivers which label distinct tuberculo-bulbar neuron subclasses defined by topology within the AOTU and BU. Each row represents a distinct Gal4 driver; first and second columns are frontal and horizontal sections labeled with *10xUAS-mCD8::GFP*, respectively. Neuropil labeled with anti-DN-cadherin (red) and axon tracts by anti-Neuroglial (blue). Third column is a single cell clone generated by MCFO using the same Gal4; white hatched lines outline neuropil compartments from the same fly. (D–F) *R88A06-Gal4* (AOTUla/c/p to BUs). (G–I) *R34H10-Gal4* (AOTUil to BUa). (J–L) *R49E09-Gal4* (AOTUim to BUi).

(M–T) Gal4 drivers which label distinct medullo-tubercular neuron subclasses defined by topology within the medulla and AOTU. (M–P) *R73C04-Gal4* labels a class of medullo-tubercular neurons projecting from m7 layer of the medulla to AOTU. (M) High

magnification image of the AOTU, (N) is the medulla from the same fly. Neuropil labeled with anti-DN-cadherin (red) and axon tracts by anti-Neuroglian (blue). (O–P) Single cell clone generated by MCFO with *R73C04-Gal4*, all panels are the same clone. Frontal section of the dendritic arborization (O) demonstrates that this cell type is not restricted to a single medulla layer. Successive tangential sections (O' and O'') reveal that the primary dendritic arborization (O'') extends multiple distal processes which occupy individual medulla columns. Neuropil labeled with anti-Brp (O–O''; red), white hatched lines outline neuropil compartments (P). (Q–R) *R56F07-Gal4* (dorsal half m7 layer to AOTUil). (J–L) *R25C04-Gal4* (dorsal half m7 layer to AOTUim).

Other abbreviations: AOT, anterior optic tract; deCP, central descending protocerebral fascicle; FB, fan shaped body; IPa, anterior inferior protocerebrum; IPm, medial inferior protocerebrum; LAL, lateral accessory lobe; LO, lobula; MEd, distal medulla; MEp, proximal medulla; ML, medial lobe of the mushroom body; PED, peduncle of the mushroom body; SLP, superior lateral protocerebrum; SP, spur of the mushroom body
Scale Bars: 25µm (A); 25µm (B–E, G, H, J, K, M, Q, S); 25µm (F, I, L); 50µm (N, R, T); 50µm (O); 20µm (O', O''); 50µm (P)

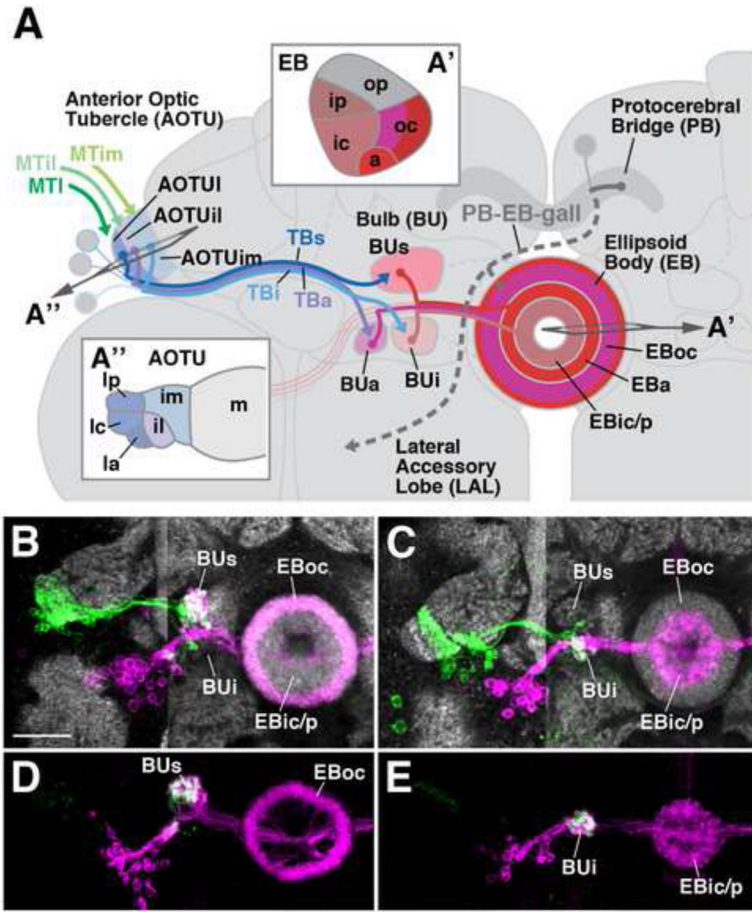


Figure 4. Framework of connectivity in the AVP - DALc1 and DALc2 provide direct, topographically-organized parallel input to ring neuron subclasses
 (A) Schematic overview of the anterior visual pathway. Insets depict horizontal sections of the EB (A') and AOTU (A'').
 (B and C) Two-color labeling of superior bulb (B) and inferior bulb (C) components. Tuberculo-bulbar neurons labeled in green by Gal4, ring neurons labeled in magenta by LexA. (B) *R88A06-Gal4* labels DALc1d tuberculo-bulbar neurons, *R19C08-LexA* labels EBoc R2 neurons; overlap observed in the superior bulb (BU_s). (C) *R49E09-Gal4* labels DALc1d tuberculo-bulbar neurons, *R54B05-LexA* labels EBic/ip R3 neurons; overlap observed in the inferior bulb (BU_i).
 (D and E) GRASP analysis of tuberculo-bulbar neuron – ring neuron synapses using the same driver combinations as B and C; post-synaptic cells are expressing CD2-RFP and split-GFP11, presynaptic cells expressing split-GFP1-10. Strong GRASP signal observed in the expected bulb subdomain.
 Scale Bars: 25µm (B–E)

Author Manuscript

Author Manuscript

Author Manuscript

Author Manuscript

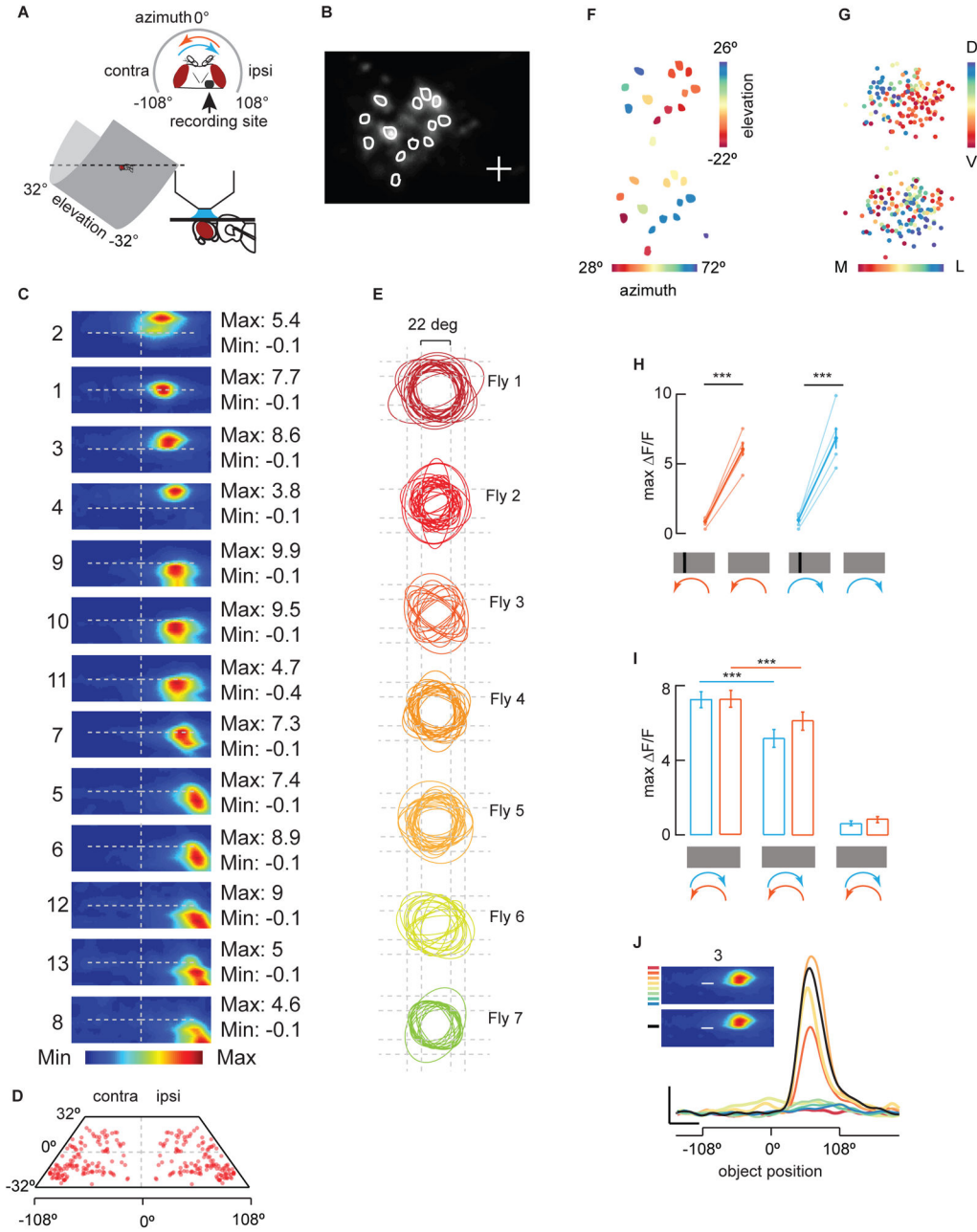


Figure 5. Physiological properties of tuberculo-bulbar neurons innervating the superior bulb
 (A) Schematic of two-photon experimental setup. Quiescent female flies are spatially fixed in front of a curved array of LEDs. The upper corners of the LED display are obscured by the mounting stage and outside the field of view (dashed line), which is reflected in the parallelogram receptive field projections in C and D below.
 (B) Two photon excitation image of a representative fly in which *R88A06-Gal4* is driving the expression of GCaMP6m in DALc11-derived tuberculo-bulbar neurons of the superior bulb (TuBu_s). All recordings are from the microglomerular presynaptic terminals of the right

bulb. Responsive microglomeruli are randomly indicated numerically as individual regions of interest (ROIs; white).

(C) For individual microglomeruli enumerated from representative fly in panel B, receptive field maps were generated using a small object passed at 8 different elevation trajectories in both directions. Maps from 13 microglomeruli are sorted from highest to lowest elevation center of the receptive field 'hotspot' (C) to indicate the visual coverage by an ensemble of receptive fields. All receptive fields are mapped from ipsilateral microglomeruli. See also Figure S1.

(D) The location of receptive field centers from all receptive field measurements (136 ROIs) from all flies (n=7) are indicated with red dots, demonstrating the coverage across the visual field. To facilitate visual comparison, receptive field centers measured from ipsilateral ROIs are reflected to the contralateral side under the presumptions of bilateral symmetry.

(E) Circumference tracings of receptive fields measured from 7 flies, 136 ROIs, demonstrate stereotypy of receptive field size across microglomeruli and across animals.

(F) The spatial arrangement of imaged microglomeruli ROIs recorded from a single fly (ROIs from panel B) are color coded according to receptive field location in elevation (top) and azimuth (bottom) to indicate retinotopic arrangement.

(G) Similar to panel F, the retinotopic distribution of microglomeruli recorded from all 7 flies and 136 microglomeruli ROIs. Each microglomerular ROI is indicated by a small uniform dot color coded as in panel F. D,V,M,L indicate dorsal, ventral, medial, lateral.

(H-I) Visual stimuli presented in both horizontal directions as shown in (A); ipsi-to-contramotion (orange) and contra-to-ipsi motion (blue). (H) Pairwise comparison between the mean of maximum F/F responses from all ROIs and all preparations to both an OFF and ON bar n=7 ($p < 0.001$, Wilcoxon signed rank test). (I) Mean of pooled peak amplitude responses relative to stimulus onset from six flies to an ON object (left), an ON bar (middle), and a wide-field grating (right). n=6. Error bars indicate S.E.M. $P < 0.001$, Wilcoxon signed rank test.

(J) Superior bulb microglomeruli do not show surround inhibition. From a single representative ROI (microglomerulus 3 from panel B), calcium responses are shown for 8 different trajectories of an ON object (color indicates elevation of horizontal sweep) by comparison to an ON bar spanning the full elevation of the display (black trace). The bar evokes nearly the same response as the object passing through the hotspot of the receptive field. Scale bar is 200% F/F and 2 seconds, y and x axis respectively.

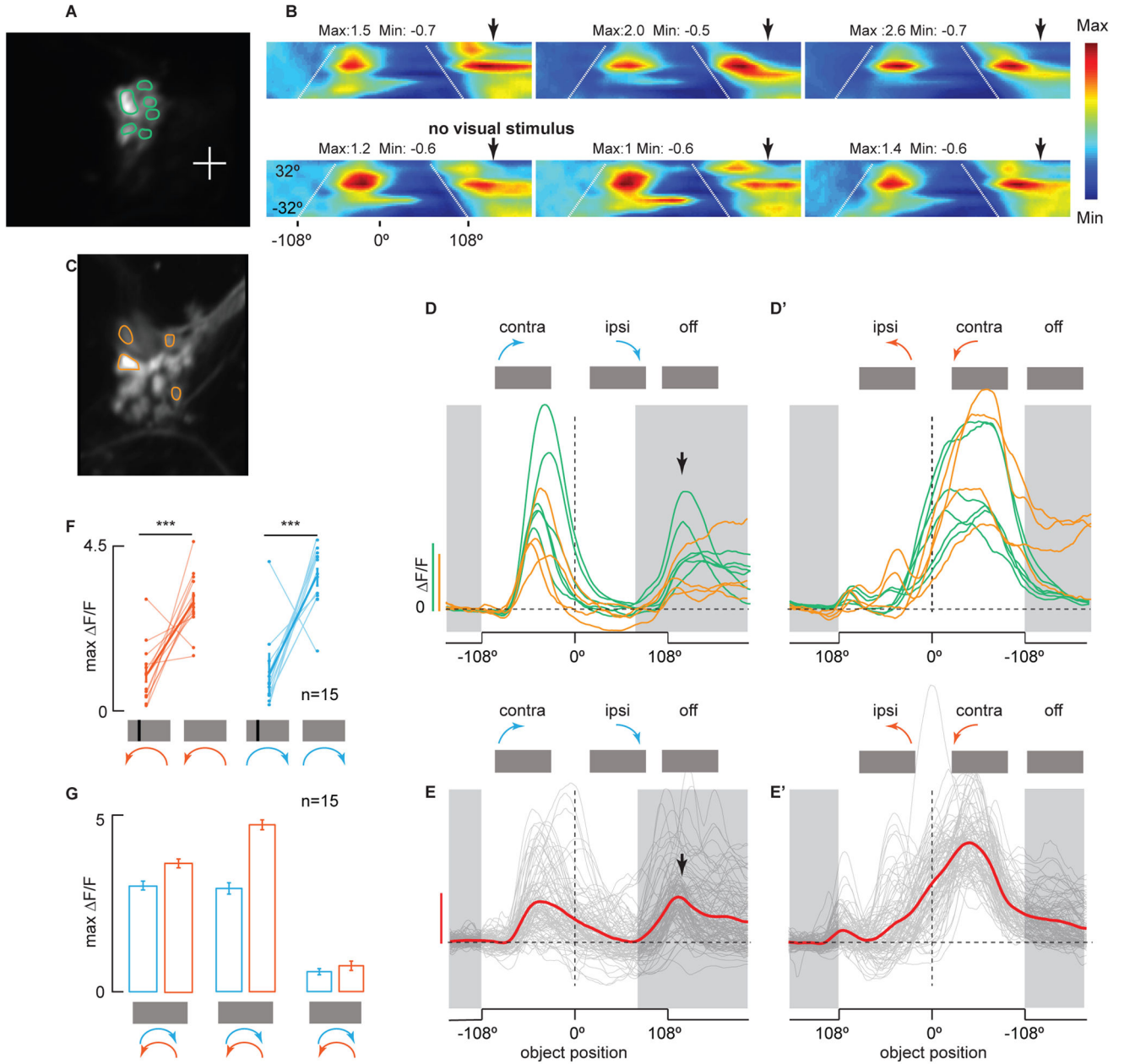


Figure 6. Physiological properties of tuberculo-bulbar neurons innervating the inferior bulb

(A–E′) Canonical responses from a subset of inferior bulb microglomeruli.

(A) Two photon excitation image of a representative fly in which *R49E09-Gal4* is driving the expression of GCaMP6m in DALcl2 tubercular-bulbar neurons of the inferior bulb (TuBu_l). Imaging plane reflects the microglomeruli (ROIs; mint green) in the dorso-posterior most position in the inferior bulb.

(B) Receptive field maps of ROIs in (A) generated by contralateral to ipsilateral (contra-to-ipsi) motion of an ON object passed at 8 different elevation trajectories. Maps demonstrate stereotypy of a class of microglomeruli typically localized to this position in the inferior bulb. Receptive fields are large and centered in the contralateral visual hemifield. Calcium

accumulation decreases for stimuli in the ipsilateral visual field as indicated by negative minimum F/F values. Note secondary excitation after the object has left the field of view (black arrows). White dashed lines indicate display boundaries.

(C) Second imaging plane from same preparation as (A) contains some microglomeruli which exhibit a canonical $TuBu_1$ response (light orange), but also many that do not (unlabeled microglomeruli).

(D–D') ON bar responses from inferior bulb microglomeruli which exhibit the canonical response described in (B) from the representative fly shown in (A–C). Responses from ROIs from the first plane (mint green) and second plane (light orange) are shown as traces from contra-to-ipsi presentation (D) and ipsilateral to contralateral (ipsi-to-contra) presentation (D') of the ON bar. Scale bars are 400% F/F for mint green and 100% F/F for light orange. Shaded grey envelopes indicate portions of the experiment when the stimulus is out of the visual field. Black arrow indicates secondary microglomeruli responses after the ON bar has left the visual field. See also Figure S2.

(E–E') Pooled population data from all ROIs and all flies, exhibiting on average distinct $TuBu_1$ response for contra-to-ipsi (E) and ipsi-to-contra (E') presentation of the ON bar. Raw traces shown in gray, mean of all traces in red. Scale bar is 200% F/F . Shaded grey envelopes and black arrow as described in D–D'. $n=15$, 104 ROIs.

(F–G) Visual stimuli presented in both horizontal directions; ipsi-to-contra motion (blue) and contra-to-ipsi motion (orange). (F) Pairwise comparison between the mean of maximum F/F responses from all ROIs which exhibit a canonical $TuBu_1$ response from each preparation; indicating ON selectivity ($n=15$, $p<0.001$, Wilcoxon signed rank test) (G) Mean of pooled peak amplitude responses relative to stimulus onset from fifteen flies to an ON object (left), an ON bar (middle), and wide-field gratings (right). $n=15$, error bars indicate S.E.M.

Table 1

Comparative terminology for central complex pathways

| Putative Homologies in other insects | Drosophila Neuron Classification | Abridged designation(s) | Subclasses | Lineage Designation |
|--|--|----------------------------|--|--|
| Transmedulla neurons, formerly line-tangential neurons | medullo-tubercular neurons | MeTu neurons | MeTu ₁ | Optic Lobe-Derived |
| | | | MeTu _{1l} | Optic Lobe-Derived |
| | | | MeTu _{1m} | Optic Lobe-Derived |
| tubercle-lateral accessory lobe neuron type 1 (TuLAL1 neurons) | tuberculo-bulbar neurons | TuBu | TuBu _s | DALc11 |
| | | | TuBu _a | DALc11 |
| | | | TuBu _i | DALc12 |
| tangential neurons of the central body lower division (TL neurons) | ring neurons | R neurons | R1, R2, R3, R4m, R4d R5 (new designation - previously unclassified) | DALv2 |
| Columnar neurons of the CBL type 1 (CL1 neurons) | protocerebral bridge- ellipsoid body- Gall neurons | PB-EB-gall (Wedge neurons) | | DM1/DPMm1, DM2/DPMpm1, DM3/DPMpm2, DM4/CM4 |
| Columnar neurons of the CBL type 2 (CL2 neurons) | protocerebral bridge- ellipsoid body- noduli neurons | PB-EB-NO (Tile neurons) | | DM1/DPMm1, DM2/DPMpm1, DM3/DPMpm2, DM4/CM4 |